ELSEVIER

Nuclear Instruments and Methods in Physics Research B 187 (2002) 87–94

NIM B
Beam Interactions with Materials & Atoms

www.elsevier.com/locate/nimb

50 MeV Li^{3+} irradiation effects on the thermal expansion of $Ca_{1-x}Sr_xZr_4P_6O_{24}$

Basavaraj Angadi [a], V.M. Jali [a,*], M.T. Lagare [a], N.S. Kini [b], A.M. Umarji [b], Ravi Kumar [c], S.K. Arora [c], D. Kanjilal [c]

[a] *Department of Physics, Gulbarga University, Gulbarga 585 106, India*
[b] *Materials Research Centre, Indian Institute of Science, Bangalore 560 012, India*
[c] *Nuclear Science Centre, New Delhi 110 067, India*

Received 22 March 2001; received in revised form 31 July 2001

Abstract

The influence of 50 MeV Li^{3+} ion irradiation on the thermal expansion of the low thermal expansion ceramic $Ca_{1-x}Sr_xZr_4P_6O_{24}$ ($x = 0.00$, 0.25, 0.50, 0.75 and 1.00) belonging to the sodium zirconium phosphate (NZP) family of ceramics was studied in the temperature range 300–1100 K. The observed changes in XRD, microstructure and thermal expansion are reported. These changes are strongly dependent upon the strontium substitution at calcium sites in the basic structure. The XRD and scanning electron microscope (SEM) studies indicate that the ion irradiation causes amorphization, especially at the grain boundaries. The thermal expansion hysteresis reduces due to Sr substitution and is further reduced upon irradiation. It is suggested that the amorphization due to irradiation helped release of thermal stress and thereby lead to the reduction in the hysteresis in thermal expansion. The composition with $x = 0.50$ having low coefficient of thermal expansion (CTE), low hysteresis and the least thermal expansion anisotropy is least affected by the Li^{3+} irradiation and hence may qualify as the radiation resistant material.

PACS: 61.82.M; 65.70; 61.80
Keywords: NZP ceramics; Low thermal expansion; Irradiation; $Ca_{1-x}Sr_xZr_4P_6O_{24}$

1. Introduction

$Ca_{1-x}Sr_xZr_4P_6O_{24}$ (CSZP) system belongs to a large structural family of new low thermal expansion materials known as sodium zirconium phosphate (NZP) family discovered by Roy and co-workers [1–3]. The members of this family have received much attention in recent times because of their very low coefficient of thermal expansion (CTE) [1,2,4], controlled lattice thermal expansion anisotropy [5,6], fast ionic conductivity [7,8], high thermal and chemical stability [9] and flexibility towards ionic substitutions [10].

The crystal structure of $NaZr_2(PO_4)_3$ consists of a rigid three-dimensional network of PO_4 tetrahedra sharing corners with ZrO_6 octahedra and

* Corresponding author.
E-mail address: vmjali@rediffmail.com (V.M. Jali).

0168-583X/02/$ - see front matter
PII: S0168-583X(01)00847-3

a three-dimensionally linked interstitial space occupied partially by Na^+ ions [11]. This partially covalently bonded three-dimensional skeletal framework is expected to show essentially low CTE although the total thermal expansion would be influenced by the interstitial ions. The tailorability of the thermal expansion of NZP materials through the careful selection of the interstitial ions and the composition provides scope for the synthesis of near zero expansion materials over any desired temperature range. Limaye et al. [6] investigated the synthesis and the thermal expansion of $MZr_4P_6O_{24}$ (M = Mg, Ca, Sr, Ba) and found that $CaZr_4P_6O_{24}$ (CZP) and $SrZr_4P_6O_{24}$ (SZP) exhibited opposing anisotropy.

It is well known that the material properties can be tailored by irradiation with energetic particles. Changes produced by ion irradiation on the physical properties of low thermal expansion materials have been investigated in order to understand the nature of radiation-induced defects in this kind of materials. A high energy heavy ion loses its energy in a medium through two processes, namely electronic loss (S_e) and nuclear collisions (S_n). The latter process is the dominant mode of energy loss at low ion energies and peaks around 1 keV/u and is responsible for displacing atoms of the medium from their lattice positions. The electronic energy loss is appreciable at higher energy and peaks around 1 MeV/u. In this process the target atom is not displaced but only excited or ionized. However, it can lead to displacement of lattice atoms in a cylindrical core along the ion path in insulating materials either through the Coulombic explosion or the thermal spike. The passage of ions through an insulator produces a positively charged cylinder, which explodes radially due to Coulomb force, causing coherent atomic movements until the ions are screened by the conduction of electrons. Due to the resulting cylindrical shock wave, which is known as the Coulomb explosion, columnar defects are formed [12]. In the other competing process kinetic energy of the electrons ejected from the target atom is transferred to the lattice by electron–phonon interaction, resulting in the increase of the local lattice temperature over the melting point of the material and is hence named as thermal spike. The temperature increase is followed by a rapid quenching, which results in an amorphous columnar structure when the melt solidifies [13]. Thus we see that both the mechanisms produce amorphous regions in the medium. Experiments have shown that when the electronic energy loss exceeds a threshold value, swift heavy ion irradiation produces an amorphous zone along the ion path in many materials [14–16].

The effects of radiation on the physical properties of low CTE materials such as silica, ULE glass, β-SiC, Astrositall, Zerodur have been reported and thermal expansion of some of them are found to be affected by the radiation [17–21]. A few radiation damage studies of low CTE glasses and glass–ceramics have also been reported [22–25]. The effect of high-energy radiation (photon or charged particle) on materials such as oxide glasses or ceramics depends upon the type and energy of the radiation and sample parameter such as temperature [26]. The solid solution CSZP is of particular interest because the composition with $x = 0.50$ shows low CTE as well as low anisotropy [6]. These factors render this into a strong ceramic suitable for many practical applications. There appear to be no reports of the effects of irradiation on the thermal expansion of NZP materials. This paper reports the effects of the 50 MeV Li^{3+} ion irradiation on structure, microstructure and thermal expansion properties of CSZP system.

2. Experimental

2.1. Synthesis

In the present work the solid solution $Ca_{1-x}Sr_xZr_4P_6O_{24}$ with $x = 0.00, 0.25, 0.50, 0.75$ and 1.00 were synthesized by conventional solid state reaction method. The stoichiometric amounts of reagent grade $CaCO_3$, $SrCO_3$, ZrO_2 and $NH_4H_2PO_4$ were used as starting materials. The calcination was carried at different temperatures in steps to drive off the volatiles and the product was then cold pressed to get samples in the form of pellets of 12 mm diameter and 0.7 mm thickness. The pellets were sintered at 1520 K for 24 h to obtain single phase.

Table 1
The electronic stopping power, S_e, nuclear stopping power, S_n, and range of 50 MeV Li^{3+} in $Ca_{1-x}Sr_xZr_4P_6O_{24}$ for samples with different compositions, x, computed using SRIM-2000 code

Composition x	$S_e = (dE/dx)_e$ (MeV/mm)	$S_n = (dE/dx)_n$ (MeV/mm)	S_e/S_n	Range (μm)
0.00	1.240×10^2	6.582×10^{-2}	1884	259.99
0.25	1.233×10^2	6.541×10^{-2}	1885	261.63
0.50	1.226×10^2	6.501×10^{-2}	1886	263.25
0.75	1.219×10^2	6.462×10^{-2}	1886	264.85
1.00	1.212×10^2	6.424×10^{-2}	1887	266.43?

2.2. Characterization

The phase identification for all the five CSZP compositions ($x = 0.00$, 0.25, 0.50, 0.75 and 1.00) was carried out by room temperature powder X-ray diffractometry using Scintag X-ray diffractometer with Cu K_α (1.5406 Å) radiation. The theoretical XRD pattern for each composition was generated by the computer code Lazy Pulverix [27] and the lattice parameter refinement was done by the linear least squares method. The microstructure of the fracture surface of the sintered specimen was obtained using Leica Cambridge Stereoscan Model S-360 scanning electron microscope (SEM). The bulk thermal expansion measurements were made using a home-built precision high temperature dilatometer [28]. Sample temperature was varied from 300 to 1100 K with heating and cooling rates of 2 K/min. Since our samples had 12 mm diameter and 0.7 mm thickness, to have better accuracy, CTE, α, was measured along the diameter of the pellet. A PC based data acquisition system recorded thermal expansion data at intervals of 120 s averaged over 10 s at each point.

2.3. Irradiation

The samples were irradiated at room temperature to 50 MeV Li^{3+} ions with a fluence of 1×10^{14} ions/cm^2 using 15 UD Pelletron at Nuclear Science Centre, New Delhi. The ion beam, incident along the axis of the pellet, was made to scan over an area of 12×12 mm^2 using magnetic scanner in order to achieve the dose uniformity across the sample area. The sample surfaces were electrically grounded to minimize the sample charging. The stopping power and range calculations for 50 MeV Li^{3+} ions in the samples used were carried using SRIM-2000 programme [29] and are shown in Table 1. We find that the range of Li^{3+} ions in the

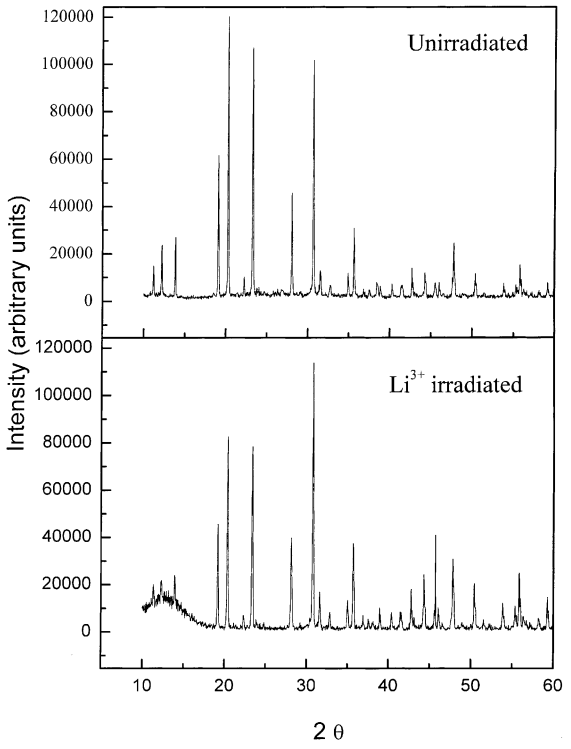

Fig. 1. XRD pattern for unirradiated and Li^{3+} irradiated SZP sample ($x = 1.00$).

samples varies from 0.26 to 0.27 mm. Since the thickness of the pellets is 0.7 mm to achieve maximum irradiation, the pellets were irradiated successively from the two faces.

3. Results and discussion

A typical XRD pattern, before and after irradiation, is shown in Fig. 1 for a CSZP sample with $x = 1$. The phase of the CSZP samples with $x = 0.00$ (CZP) and $x = 1.00$ (SZP) were confirmed by comparing their XRD patterns with the standard JCPDS patterns No. 33-321 and No. 33-1360, respectively. All the five compositions in the CSZP system could be indexed on a hexagonal lattice ($R\bar{3}C$). The lattice parameters for both the unirradiated and the irradiated samples are calculated by the linear least squares method and are shown in Table 2. We see that lattice parameters for

Table 2
Lattice parameters (a and c) and CTE, α, for samples with different compositions, x

Composition x	a (Å)		c (Å)		CTE (K^{-1})		$\Delta\alpha \times 10^6$ (K^{-1})
	Unirradiated	Irradiated	Unirradiated	Irradiated	$\alpha_{un} \times 10^6$	$\alpha_{irr} \times 10^6$	
0.00	8.785(5)	8.772(5)	22.693(14)	22.652(13)	−1.77	−0.12	1.65
0.25	8.758(5)	8.756(5)	22.920(14)	22.824(13)	0.85	1.81	0.96
0.50	8.729(4)	8.730(5)	23.119(13)	23.055(13)	1.66	1.69	0.03
0.75	8.720(4)	8.712(5)	23.232(14)	23.202(14)	2.32	2.27	0.05
1.00	8.701(5)	8.647(5)	23.390(13)	23.233(13)	2.64	3.15	0.51?

α_{un} = CTE for unirradiated sample, α_{irr} = CTE for irradiated sample and $\Delta\alpha = |\alpha_{irr} - \alpha_{un}|$ = change in α due to irradiation.

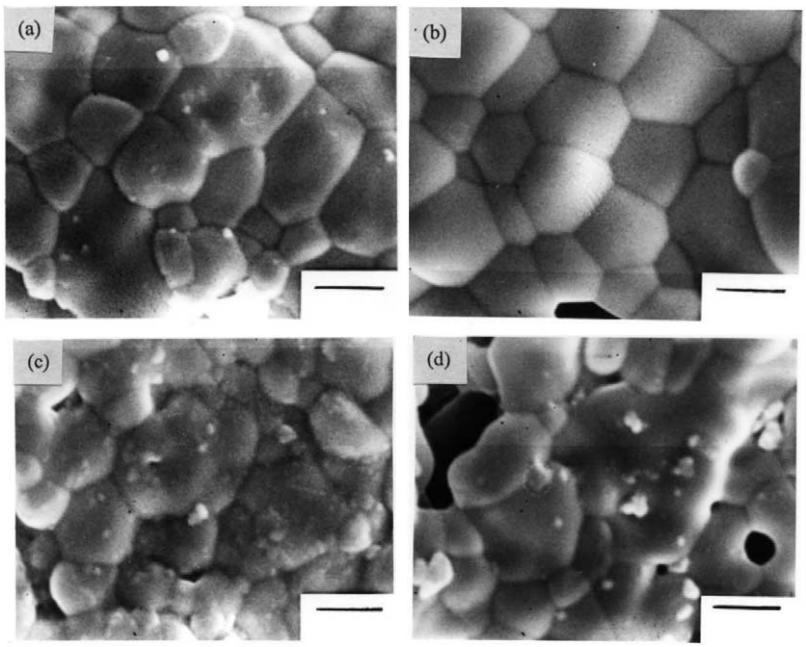

Fig. 2. SEM Photographs for $x = 0.00$ composition: (a) before irradiation; (c) after irradiation and for $x = 0.50$ composition: (b) before irradiation; (d) after irradiation. Bar = 2 μm.

unirradiated samples agree with reported values and that these do not change substantially due to irradiation. In Fig. 1 lower 2θ side of the XRD pattern of the irradiated samples shows diffuse nature, which is indicative of presence of amorphous material. The appearance of crystalline peaks over the amorphous background, shows that the irradiation has produced some amount of amorphous material having the crystal structure same as the unirradiated material as can be seen from the lattice parameters shown in Table 2.

The SEM microstructure analysis of the unirradiated samples with $x = 0.00$ and 0.50, shown in Figs. 2(a) and (b) respectively, indicates the presence of single phase and dense grains with an average grain size $\sim$2.47 μm having sharp grain boundaries. The SEM pictures of these samples after irradiation, in Figs. 2(c) and (d) respectively, show no apparent change in the grain size but present blurred grain boundaries. This implies that, due to irradiation, while there is no change in grain structure there is some amorphization at the grain boundaries. This can be attributed to the fact that the weak grain boundary region is susceptible for damage due to energy deposition by ions.

The thermal expansion plots recorded during heating and cooling cycles for the five compositions before and after irradiation are shown in Figs. 3–7. The area of these hysteresis curves as a function of the respective composition is shown in Fig. 8. It may be noticed that, in the case of unirradiated samples, the $x = 0.00$ composition shows appreciable hysteresis and the $x = 0.50$ composition has minimum hysteresis. It is interesting to note that there is a further decrease in the hysteresis after irradiation in each of the compositions. The hysteresis is related to the thermal stress built up in the sample due to thermal expansion anisotropy and the release of these stresses manifests in the thermal expansion hysteresis. It is

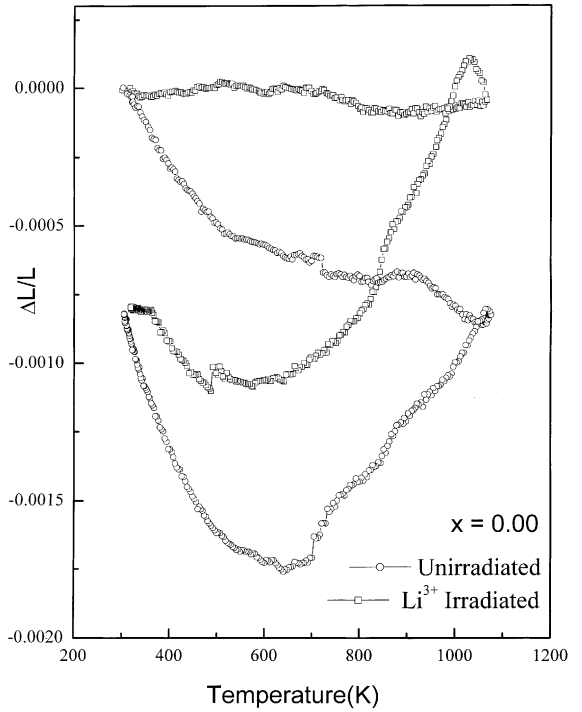

Fig. 3. Thermal expansion plots for unirradiated and Li^{3+} irradiated sample with $x = 0.00$ composition.

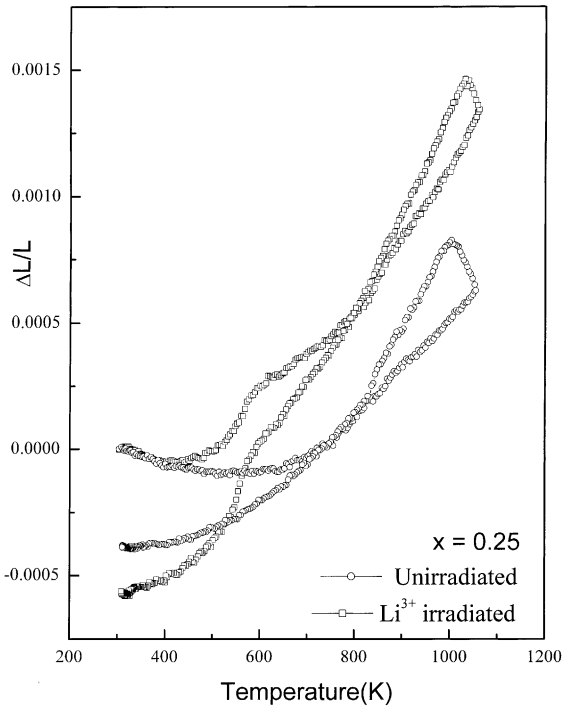

Fig. 4. Thermal expansion plots for unirradiated and Li^{3+} irradiated sample with $x = 0.25$ composition.

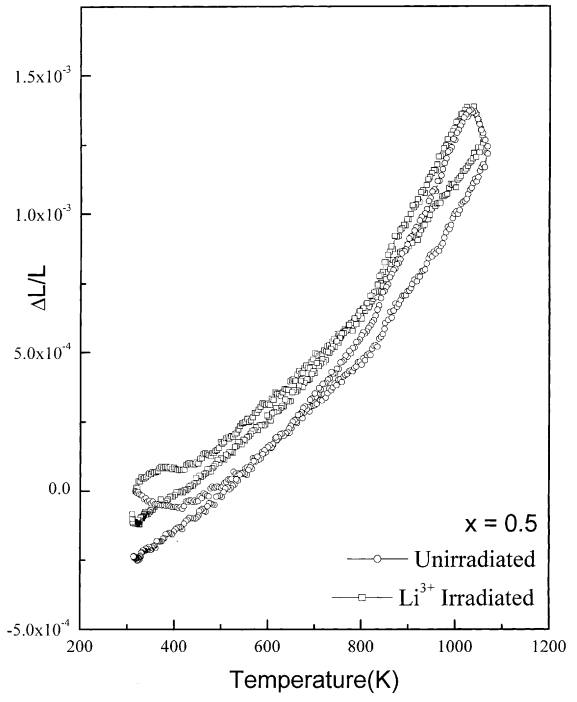

Fig. 5. Thermal expansion plots for unirradiated and Li^{3+} irradiated sample with $x = 0.50$ composition.

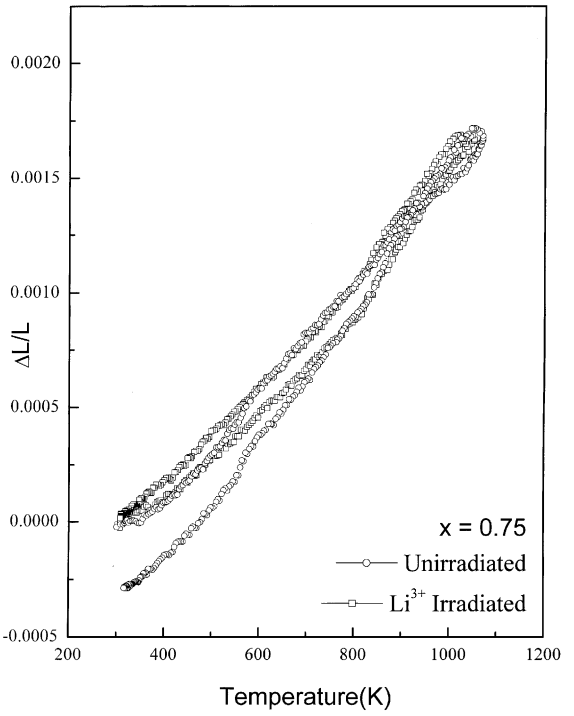

Fig. 6. Thermal expansion plots for unirradiated and Li^{3+} irradiated sample with $x = 0.75$ composition.

known that microcrack formation is due to the stresses associated with the axial thermal expansion anisotropy and it is dependent upon the grain size. The effective grain size for $x = 0.00$ composition is above the critical grain size for microcracking to occur whereas for the remaining samples it is below this value. Hence we may expect appreciable stress release through microcracking and the resultant hysteresis only in $x = 0.00$ sample. This qualitatively explains the observed decrease in the hysteresis in the rest of samples. To explain the further decrease in hysteresis after irradiation we may invoke the other possible mechanism for the release of the stresses. It is possible that the amorphous material produced by irradiation, and seen in SEM pictures at the grain boundaries, may undergo viscous flow to relieve the thermal stresses.

The average values of α in the temperature region from 300 to 1100 K obtained from the thermal expansion plots are shown in Table 2 and are plotted as a function of x in Fig. 9. It may be noticed that the average α for unirradiated samples increases progressively from negative (contracting) to positive value (expanding) as we go from $x = 0.00$ to $x = 1.00$ compositions in the solid solution CSZP. The composition with $x = 0.50$ deserves special attention as it has nearly zero average α. The observed changes in α may be understood in terms of change in the chemical composition. The Ca–O bond in CZP and the Sr–O bond in SZP are mainly responsible for the thermal expansion behavior in these materials. Further, as said earlier, since the CZP and SZP show opposing anisotropy, gradual substitution of larger Sr in the place of Ca sites in the basic structure of CZP brings about the observed change in α and leads to the low thermal expanding material for $x = 0.50$. The average α for irradiated samples also shows similar behavior but the actual values for $x = 0.00$, 0.25 are higher than those for the unirradiated sample. Fig. 9 also shows change in α due to irradiation for the five

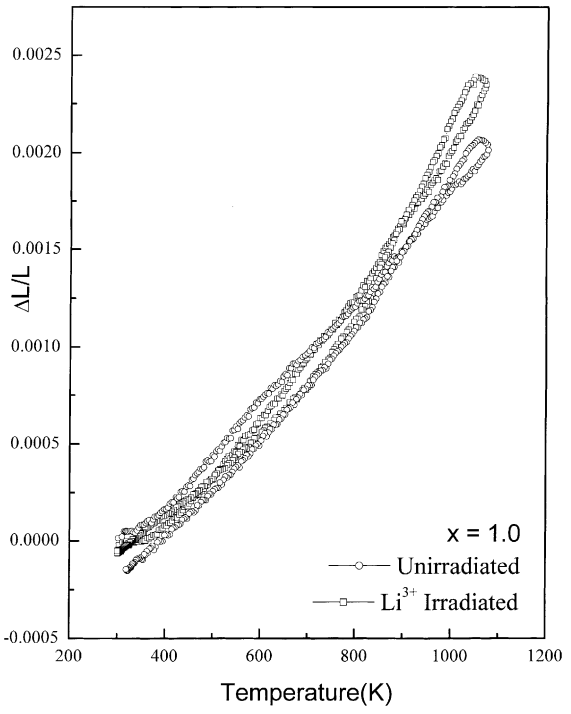

Fig. 7. Thermal expansion plots for unirradiated and Li^{3+} irradiated sample with $x = 1.00$ composition.

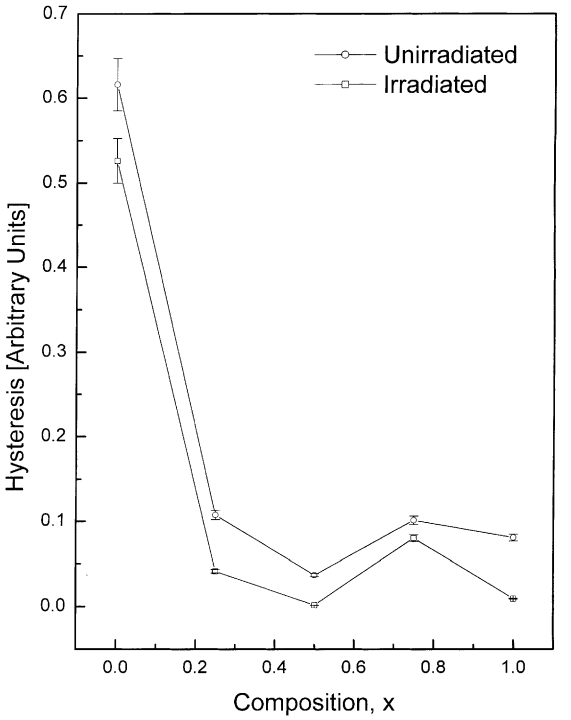

Fig. 8. Variation of areas of the hysteresis curves (Fig. 3–7) with the composition, x.

compositions. It can be seen that the change in α due to irradiation decreases with composition (x), reaches a minimum for $x = 0.50$ and then slightly increases. The $x = 0.00$ composition which was contracting before irradiation becomes almost zero expanding after Li^{3+} irradiation. The composition with $x = 0.50$ having low CTE and least thermal expansion anisotropy is least affected by the Li^{3+} irradiation compared to other compositions and hence can be considered as a radiation resistant material. We may understand the irradiation effects on α in terms of mode of energy loss of the Li^{3+} ions. From Table 1 we see that the electronic stopping power, S_e, is about three orders of magnitude greater than the nuclear stopper power, S_n. In fact, the value of S_n is about 0.065 eV/nm, and is too small to create displacement damage in the materials. Hence radiation induced changes in α are to be attributed to the amorphization produced by S_e through thermal spike or Coulomb explosion.

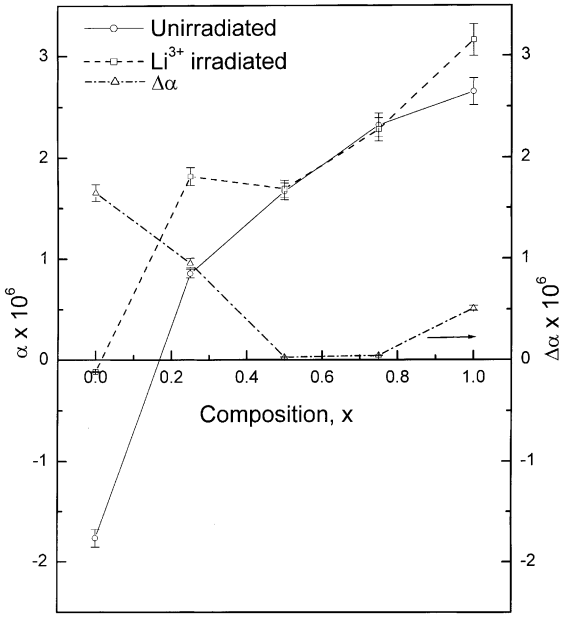

Fig. 9. Variation of CTE, α, and change in α due to irradiation, $\Delta\alpha$, with composition, x. α_{un} = CTE for unirradiated sample, α_{irr} = CTE for irradiated sample and $\Delta\alpha = |\alpha_{irr} - \alpha_{un}|$.

Acknowledgements

The stable high quality ion beam provided by the Pelletron group at the Nuclear Science Centre, New Delhi and the financial assistance from this center under the UFUP grant No. 2303 are gratefully acknowledged.

References

[1] J. Alamo, R. Roy, J. Am. Ceram. Soc. 67 (1984) C78.
[2] R. Roy, D.K. Agrawal, J. Alamo, R.A. Roy, Mater. Res. Bull. 19 (1984) 471.
[3] D.K. Agrawal, V.S. Stubican, Mater. Res. Bull. 20 (1985) 99.
[4] G.E. Lenain, H.A. McKinstry, S.Y. Limaye, A. Woodward, Mater. Res. Bull. 19 (1984) 1451.
[5] T. Oota, I. Yamai, J. Am. Ceram. Soc. 69 (1986) 1.
[6] S.Y. Limaye, D.K. Agrawal, H.A. McKinstry, J. Am. Ceram. Soc. 70 (1987) C232.
[7] J.B. Goodenough, H.Y-P. Hong, J.A. Kofalas, Mater. Res. Bull. 11 (1976) 203.
[8] H.Y-P. Hong, Mater. Res. Bull. 11 (1976) 173.
[9] G. Harshe, D.K. Agrawal, S.Y. Limaye, J. Am. Ceram. Soc. 77 (1994) 1965.
[10] J. Alamo, R. Roy, J. Mater. Sci. 21 (1986) 444.
[11] L. Hagman, P. Kierkegaard, Acta Chem. Scand. 22 (1968) 1822.
[12] D. Lesueur, A. Dunlop, Radiat. Eff. Def. Solids 126 (1993) 163.
[13] G. Szenes, Phys. Rev. B. 51 (1995) 8026.
[14] F. Studer, C. Houpert, H. Pascard, R. Spohr, J. Vetter, J-Y. Fan, M. Toulemonde, Radiat. Eff. Def. Solids 116 (1991) 59.
[15] M. Toulemonde, S. Bouffard, F. Studer, Nucl. Instr. and Meth. B 91 (1994) 108.
[16] J. Provost, C. Simon, M. Hervieu, D. Groult, V. Hardy, F. Studer, M. Toulemonde, MRS Bull. 20 (1995) 22.
[17] E. Lell, N.J. Kreidl, J.R. Hensler, in: J.E. Burke (Ed.), Progress in Ceramic Science, Vol. 4, Pergamon, New York, 1966, p. 1.
[18] E.J. Friebele, D.L. Griscom, in: M. TomozawaR.H. Doremus (Eds.), Treatise on Materials Science and Technology, Glass II, Vol. 17, Academic Press, New York, 1979, p. 257.
[19] R. Bruckner, J. Non-Cryst. Solids 5 (1970) 123.
[20] R. Bruckner, J. Non-Cryst. Solids 6 (1971) 177.
[21] N. Koumvakalis, M.G. Jani, L.E. Halliburton, Appl. Opt. 25 (1986) 4288.
[22] S.M. Brekhovskikh, Yu.L. Grinshtein, Glass–Ceram., N.Y. Consult. Bur. Trans. 22 (1965) 517.
[23] D.L. Porter, M.R. Pascucci, B.H. Olbert, J. Nucl. Mater. 103 (1981) 767.
[24] T.E. Tsai, P.L. Higby, E.J. Friebele, D.L. Griscom, J. Appl. Phys. 62 (1987) 3488.
[25] P.L. Higby, E.J. Friebele, C.M. Shaw, M. Rajaram, E.K. Graham, D.L. Kinser, E.G. Wolff, J. Am. Ceram. Soc. 71 (1988) 796.
[26] M. Rajaram, E.J. Friebele, J. Non-Cryst. Solids 108 (1989) 1.
[27] R. Yvon, J. Wolfgang, P. Ervin, J. Appl. Cryst. 10 (1977) 73.
[28] A.M. Umarji, S. Senbhagaraman, M.V. Radhika Rao, J. Instr. Soc. India 27 (1997) 109.
[29] J.F. Ziegler, J.P. Biersack, U. Littmark, in: The Stopping and Ranges of Ions in Solids, Pergamon, New York, 1985, New edition, 1999.